Arabian Journal of Chemistry (2017) xxx, xxx–xxx

King Saud University

Arabian Journal of Chemistry

www.ksu.edu.sa
www.sciencedirect.com

REVIEW

New CaO-based adsorbents prepared by solution combustion and high-energy ball-milling processes for CO_2 adsorption: Textural and structural influences

Abel Granados-Pichardo [a,b], Francisco Granados-Correa [a,*], Víctor Sánchez-Mendieta [b], Héctor Hernández-Mendoza [a]

[a] *Departamento de Química, Instituto Nacional de Investigaciones Nucleares, A.P. 18-1027, Col. Escandón, Delegación Miguel Hidalgo, C.P. 11801 Cd. de México, Mexico*
[b] *Facultad de Química, Universidad Autónoma del Estado de México, Paseo Colón y Tollocan s/n, C.P. 50000 Toluca, Estado de México, Mexico*

Received 30 November 2016; accepted 15 March 2017

KEYWORDS

CaO-based adsorbents;
CO_2 capture;
Solution combustion synthesis;
Ball-milling process;
Textural properties;
Structural influences

Abstract In the present work, new CaO-based adsorbents were obtained by a fast solution combustion method and high-energy ball-milling process to study their CO_2 capture behavior under different moderate pressure and temperature conditions. The as-prepared CaO products were characterized systematically using different analytical techniques such as X-ray diffraction, scanning electron microscopy and N_2 physisorption measurements. The results showed that the CaO prepared by solution combustion and ball-milled during 2.5 h showed the maximum CO_2 adsorption capacity of 9.31 mmol/g at 25 °C and 1 atm mainly via chemisorption with $CaCO_3$ formation, which was corroborated by infrared spectroscopy, X-ray diffraction, and X-ray photoelectron spectroscopy studies. In general, the obtained results revealed that the synthesized CaO nanopowders from solution combustion that were treated by high-energy ball-milling enhanced their CO_2 adsorption capacity due to improved structural and textural properties, and this CaO-based adsorbent can be used as a promising material for CO_2 capture in post-combustion CO_2 capture technologies on a large scale, under atmospheric pressure and temperature conditions.

* Corresponding author.
E-mail address: francisco.granados@inin.gob.mx (F. Granados-Correa).
Peer review under responsibility of King Saud University.

Production and hosting by Elsevier

http://dx.doi.org/10.1016/j.arabjc.2017.03.005
1878-5352 © 2017 The Authors. Production and hosting by Elsevier B.V. on behalf of King Saud University.
This is an open access article under the CC BY-NC-ND license (http://creativecommons.org/licenses/by-nc-nd/4.0/).

Contents

1. Introduction

It is well known that atmospheric carbon dioxide (CO_2) concentrations have increased over the last several decades and exceeded 400 ppm (McCarthy et al., 2001). As expected, the higher atmospheric CO_2 levels have caused severe climate change, which negatively affects the environment and ecosystems (Alexeeva and Anger, 2015). In facts, the reduction of global CO_2 emissions should significantly decrease their atmosphere concentrations. Thus, developing effective methods for CO_2 mitigation is urgent. In this scenario, currently, the most promising technology for efficient CO_2 capture from flue gas stream of power plants, oil refineries, petrochemical industries, transportation sectors, and others at a great scale is based mainly on CO_2 adsorption on porous solid adsorbents. One approach of this adsorption technology is to produce a concentrated stream of CO_2 at higher pressures that can be transported readily to a storage site. Consequently, the CO_2 adsorption of solid adsorbents technology is of immense importance due to its high CO_2 adsorption capacities, suitability for batch and continuous processes, high possibility of regeneration, potential reuse, and low energy requirement (Ben-Mansour et al., 2016; Sayari et al., 2011).

Therefore, the adsorbents' physicochemical properties are crucial to the CO_2 capture technologies' practicality. In this context, several materials have been studied as promising solid adsorbents for CO_2 capture, such as activated carbons (García et al., 2011), zeolites (Hennessy, 2015), metal organic frameworks (MOFs) (Belmabkhout et al., 2016; Bhatt et al., 2016; Hou et al., 2013), zirconates (Ibarahim et al., 2015), silicates (Khomane et al., 2006; Datta et al., 2015), metal oxides (Dou et al., 2010), and polymers (Drage et al., 2009), among others. In this order, each studied solid adsorbent has provided significant improvements in both cost and performance for CO_2 capture. Now, the production of high-performance ceramic powders using different synthetic chemical and physical routes always has been an essential requirement to obtain materials with desired structural and surface properties; for example, adsorbent particle studies in controlled environments that depict the CO_2 capture conditions are another key part of the CO_2 capture process development, such as using a fluidized bed with ultrafine nanopowders for CO_2 capture technologies , that promotes the gas-solid contact (Ammendola et al., 2015; Raganati et al., 2014; Raganati et al., 2015). Among all these above solid adsorbents listed, recently metallic oxides are attractive because of their abundance, easy accessibility, and favorable thermodynamic properties. Indeed, these metallic materials have been good adsorbents for CO_2 due to their low regeneration-energy requirement and low operating temperature (Duan and Sorescu, 2010). In this scenario, both the physical and chemical properties of metallic oxide adsorbents can be used for efficient CO_2 capture, and many studies have demonstrated their reactivity for CO_2 under higher and ambient pressure and temperature conditions of flue gases (Feron, 2010; Florin and Fennell, 2011; Kavosh et al., 2015; Li et al., 2014; Ridha et al., 2015). It is well known that alkaline earth metal oxides (e.g., CaO and MgO) can react with CO_2 to form carbonates at high temperatures, and that when are heated, these metal carbonates liberate the pure stream of CO_2 gas, which can be stored and subsequently used for various technological applications. In this context, CaO has been widely recognized as a versatile solid adsorbent and can be widely used in CO_2 capture technologies due to its good selective adsorption characteristics (Lu et al., 2015). Hence, porous solid adsorbents with higher CO_2 adsorption capacity and selectivity are of utmost importance, because porous and nanosized materials present abundant nanopores or surface-active sites, which could act as determinants in CO_2 adsorption processes (Liu et al., 2008). Moreover, many CaO-based adsorbents have been considered as potential candidates for CO_2 capture because of their relatively low cost, high availability, fast kinetics, high CO_2 capture capacity, abundance, and relatively inexpensive material consumption (Feng et al., 2006; Florin and Fennell, 2011). Overall, the CO_2 capture abilities of CaO-based adsorbents have been reported widely, and researchers have stated that this material is a potential adsorbent to remove CO_2 from the atmosphere (Pacciani et al., 2008; Radfarnia and Iliuta, 2013; Valverde, 2013). Besides this, several studies have found a close relation between the carbonation rate and the porosity and crystalline structure of the CaO compounds (Lee et al., 2015a, 2015b; Lu et al., 2006; Manovic and Anthony, 2008; Ridha et al., 2015; Rouchon et al., 2013; Yang et al., 2009; Zamboni et al., 2011; Zhang et al., 2013).

On the other hand, solution combustion synthesis is a method widely used for preparing different oxide powders with high yield, high surface areas, low density and quality mesoporous structures at short times compared to other conventional synthesis methods such as calcination and precipitation, between others, that required many hours or even days to complete reactions (Mimani and Patil, 2001). Furthermore, this method is versatile, safe, simple and instantaneous for the facile fabrication of a variety of nanosized materials; moreover, the combustion synthesis requires simple equipment with energy saving (Toniolo et al., 2010). Nevertheless, this method required high temperatures for achieving the metallic salt and organic fuel decomposition through an exothermic redox reaction for the final product formation (Bhatta et al., 2015; Granados-Correa et al., 2008; Hwang and Wu, 2004). Therefore, materials prepared by the solution combustion method have attracted increasing interest because of their novel characteristics necessary for adsorption technological applications. On the other hand, it is also well known that the mechanical milling, is a

Please cite this article in press as: Granados-Pichardo, A. et al., New CaO-based adsorbents prepared by solution combustion and high-energy ball-milling processes for CO_2 adsorption: Textural and structural influences2 adsorption –>. Arabian Journal of Chemistry (2017), http://dx.doi.org/10.1016/j.arabjc.2017.03.005

method widely used to obtain nanostructure materials of reduced particle size (< 100 nm); in particular these nanoparticles present unique properties arising from their very small primary particle size and very large surface area per unit mass, and nanoparticles provide higher contact and reactions efficiencies than traditional materials (Hakim et al., 2005); moreover, mechanical-milling process allows to activate dry solids that can improve their adsorption properties (Granados-Correa et al., 2016; Janusz et al., 2010). Therefore, nanopowders show substantially enhanced adsorption characteristics superior than those of the conventionally prepared materials (Liang et al., 2001). It is important to note that the gas adsorption efficiency can increase with a decrease in the CaO powder size and crystallites. Indeed, the high gas adsorption efficiency of nanoparticles can be also caused by their structural defects on their surface.

Despite the overwhelming evidence supporting the efficient CO_2 capture abilities of CaO-based adsorbents, there is no concrete study on their CO_2 capture performance after being treated by high-energy ball milling. Then, in this work, a series of CO_2 adsorption experiments at different moderate temperatures and pressures on a series of different CaO-based adsorbents with structures and textures suitable for CO_2 adsorption were examined to study and improve adsorbent particle reactivity that can help to enhance the CO_2 capture efficiency. This study also describes the adsorbents' textural and structural influences.

2. Experimental

2.1. Materials

To obtain CaO-based adsorbents, analytic-grade reagents were employed and calcium nitrate tetrahydrate $Ca(NO_3)_24H_2O$ (98%, MERCK) and urea NH_2CONH_2 (99.9%, Sigma-Aldrich) were used as chemical precursors without further purification. In addition, distilled water was used to prepare all solutions. Calcium nitrate was employed as the precursor agent for CaO synthesis by solution combustion because metal nitrates are known for their oxidizing properties, high solubility in water, low fusion temperature, and low cost. Urea was used as an organic chemical fuel because it has the advantage of being commercially available and relatively inexpensive while offering high heat generation in the production of various ceramic powders, for a variety of advanced applications (Aruna and Mukasian, 2008). For the high-energy ball milling, Ni powder (≥99.5%, MERCK) and Fe powder (≥99.5%, MERCK) were employed. The CO_2 adsorption experiments were carried out using an ultra-dry CO_2 gas of 99.8% of purity, provided by Infra México.

2.2. CaO-based adsorbents preparation

In order to obtain new nanosized CaO-based adsorbents with large specific surface areas and high-porosity structures, the solution combustion method and ball-milling process were used. The solution combustion method, only requires a short reaction time, and is based on the explosive decomposition of urea as chemical fuel, which produces heat at higher temperatures (Granados-Correa et al., 2008). For this purpose, different molar ratios of the chemical precursors, calcium nitrate to urea (1:1–1:2.5), were tested. Then, the calculated grams of chemical precursors were mixed homogeneously in a 50 mL porcelain crucible with 1 mL of distilled water; the mixture was heated by an electrical grid to evaporate the water, which produced a solid-gel material. Finally, the obtained solid-gel was calcined at 800 °C over 5 min in a muffle furnace with 1 mL of distilled water added before calcination. The prepared solid was stored for further characterization and CO_2 capture experiments. On the other hand, the CaO sample prepared via solution combustion was treated using a ball-milling process, over different previously set times (2.5, 5.0, 7.5, and 10 h) under an argon atmosphere, using a high-energy mechanical mill of 50 mL capacity (Spex 8000 type with tungsten carbide container designed at the National Institute of Nuclear Research). In all mechanical milling runs, a ball-to-powder weight ratio of 6:1 (using 15 balls 1 mm in diameter with a total weight range of 2.5–15 g of sample) was employed. The high-energy ball-milling process also was used to obtain CaO-Fe and CaO-Ni nanocomposites using the CaO obtained by solution combustion as a bulk-material-to-pure-metal ratio of 98:2 weight percentage for Fe and Ni, respectively. The evolution of the obtained materials' important textural characteristics was monitored using N_2 physisorption measurements and X-ray diffraction. Consequently, the best physicochemical properties of materials were chosen for CO_2 adsorption experiments.

2.3. CaO-based adsorbents characterization

CaO-based adsorbents were physicochemically characterized using different analytical techniques: X-ray diffraction (XRD), N_2-physisorption measurements, and scanning electron microscopy with energy-dispersive X-ray spectroscopy (SEM-EDS). To obtain the crystalline characteristics of the prepared CaO-based adsorbents, a Siemens D-5000 X-ray diffractometer was employed using $Cu\mathrm{K}\alpha$ radiation operated at 40 kV with an angular sweep interval of 30–100° in 2θ and a sweep rate of 0.03°/s for its lattice parameter. The obtained XRD patterns were compared with the reported Joint Committee on Powder Diffraction Standards (JCPDS) cards. The crystallite sizes were determined using the Scherrer equation from the prime peak width reflections with considerable intensities (Patterson, 1939). Brunauer-Emmett-Teller (BET) specific surface areas, mean pore diameters, total pore volumes, and N_2 adsorption/desorption isotherms of the CaO-based adsorbents were determined by nitrogen physisorption measurements using BEL Japan INC model Belsorp Max equipment at 77 K. Prior to the measurements, the samples were outgassed under N_2 gas flux at 300 °C for 3 h. In addition, the pore-size distribution was estimated using the Barrett-Joyner-Halenda (BJH) method (Barrett et al., 1951). The size and shape of the obtained particles were investigated by SEM using a high vacuum electron microscope: JEOL JMS-5900 LV at 25 kV equipped with a microprobe (EDS Oxford). For better characterization, all solid samples were placed on a carbon-type aluminum holder and covered with a gold layer for 2 min, using a Denton Vacuum Desk II platter. The materials' chemical composition was determined by EDS analysis. In addition, to corroborate the formation of $CaCO_3$ in the CO_2 adsorption process, a systematic characterization of the best CaO-based adsorbent material after CO_2 capture was carried out. Additionally, Fourier transform infrared (FTIR) spectra were obtained using a Nicolette 550 spectrometer with a conventional method KBr disk in the range of 400–4000 cm^{-1}. The sample consisted of a CaO sample obtained by solution combustion at 800 °C and treated by

Please cite this article in press as: Granados-Pichardo, A. et al., New CaO-based adsorbents prepared by solution combustion and high-energy ball-milling processes for CO_2 adsorption: Textural and structural influences2 adsorption –>. Arabian Journal of Chemistry (2017), http://dx.doi.org/10.1016/j.arabjc.2017.03.005

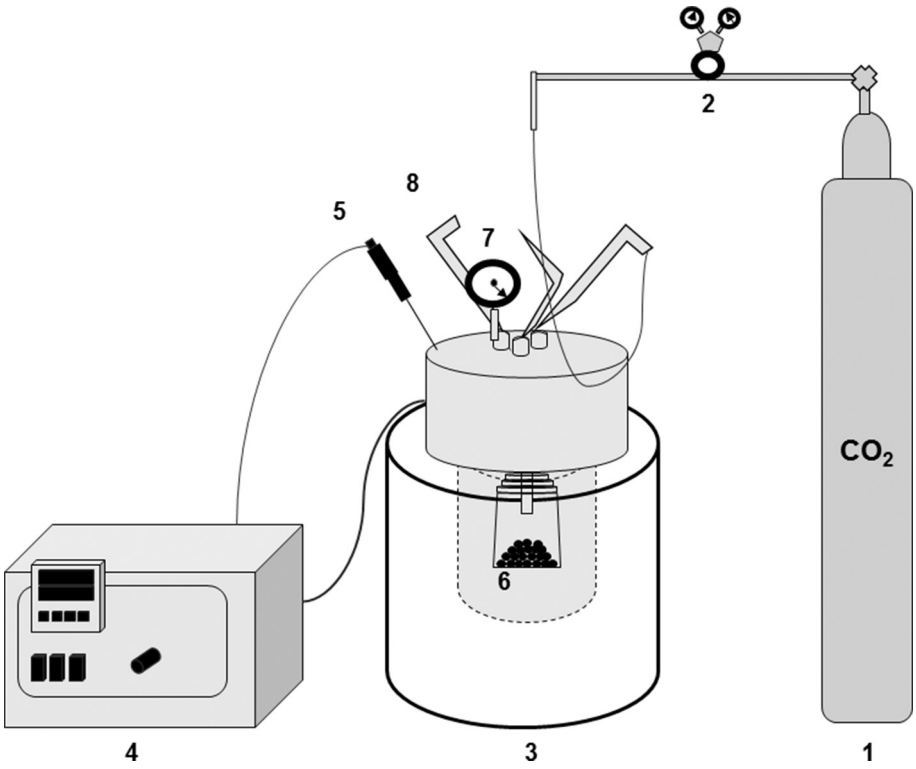

Figure 1 Schematic diagram of the CO_2 adsorption experimental setup. (1) CO_2 cylinder; (2) flow controller; (3) steel high vacuum reactor; (4) temperature controller; (5) thermocouple; (6) adsorbent; (7) pressure controller; (8) vacuum.

high-energy ball-milling over 2.5 h without any pretreatment, a CaO-BM degassed sample, and CaO-BM after the CO_2 adsorption process at 25 °C and 1 atm. On the other hand, X-ray photoelectron spectroscopy (XPS) measurements of the CaO-BM-CO_2 adsorbent were performed using a XPS Thermo Scientific K-Alpha equipment with monochromatic Al $K\alpha$ (1486 eV) radiation in a high vacuum in the range 1×10^{-10} to 1×10^{-9} mbar. The samples were analyzed at the catalyst chamber pressure at 1×10^{-9} mbar, with C1s at 285 eV as reference.

2.4. CO_2 adsorption experiments

CO_2 adsorption experiments were carried out using a steel high vacuum reactor with a 50 mL capacity designed in the ININ (Fig. 1). 8 mg of obtained CaO-based adsorbents was used in each experiment with a flue of ultra-dry CO_2 gas. The samples were put into the reactor chamber and heated to 300 °C for 30 min to eliminate the small quantity of impurities that could adhere to the samples when they were exposed to the atmosphere, since CaO is carbonized easily to form $CaCO_3$ when exposed to ambient air. To obtain the best CO_2 adsorption parameters, CO_2 adsorption experiments were carried out at different temperatures (25, 50, 75, and 100 °C), and pressures (1, 5, 10, and 15 atm), using 15-min of equilibrium contact time. The CO_2 adsorption capacity in millimoles of CO_2 adsorbed per gram of adsorbent (mmol/g) was measured using thermogravimetric and differential scanning calorimetry (TGA-DSC) analysis with an SDT Q600 calorimeter coupled to a discovery mass spectrophotometer instrument (TA Instruments-Waters) by measuring the weight loss of CO_2 that was adsorbed in the nanocompounds. The samples were heating at a rate of 20 °C/min up to 850 °C in helium atmosphere at a flow rate of 100 mL/min.

3. Results and discussion

Solution combustion and high-energy ball-milling processes were employed to produce different potential CaO-based adsorbents for efficient CO_2 capture successfully, taking into consideration their improved textural properties (e.g., specific surface area, total pore volume, and narrow pore size distribution). It is important to mention that all the derived CaO-based adsorbents from combustion solution and high-energy ball-milling processes were texturally characterized systematically considering their different preparation parameters, such as molar relation of chemical precursors-urea and calcium nitrate-for synthesis method and ball-milling time by mechanical process. Therefore, one set of four best-obtained textural CaO-based adsorbents were chosen and are referred in this work as follows: (CaO-CS) for CaO prepared by solution combustion using a ratio molar of chemical precursors-urea to calcium nitrate (2:1)-with 1 mL of distilled water before to calcination at 800 °C by 5 min, (CaO-BM) for CaO-CS treated by high-energy ball-milling over 2.5 h, (CaO-Fe) for CaO-CS doped with Fe by high-energy ball-milling over 10 h, and (CaO-Ni) for CaO-CS doped with Ni by high-energy ball-milling over 5 h. These four-solution combustion and ball-milled CaO-based samples were discussed in terms of the most significant textural and structural characteristic influences on their CO_2 adsorption behavior.

Please cite this article in press as: Granados-Pichardo, A. et al., New CaO-based adsorbents prepared by solution combustion and high-energy ball-milling processes for CO_2 adsorption: Textural and structural influences2 adsorption –>. Arabian Journal of Chemistry (2017), http://dx.doi.org/10.1016/j.arabjc.2017.03.005

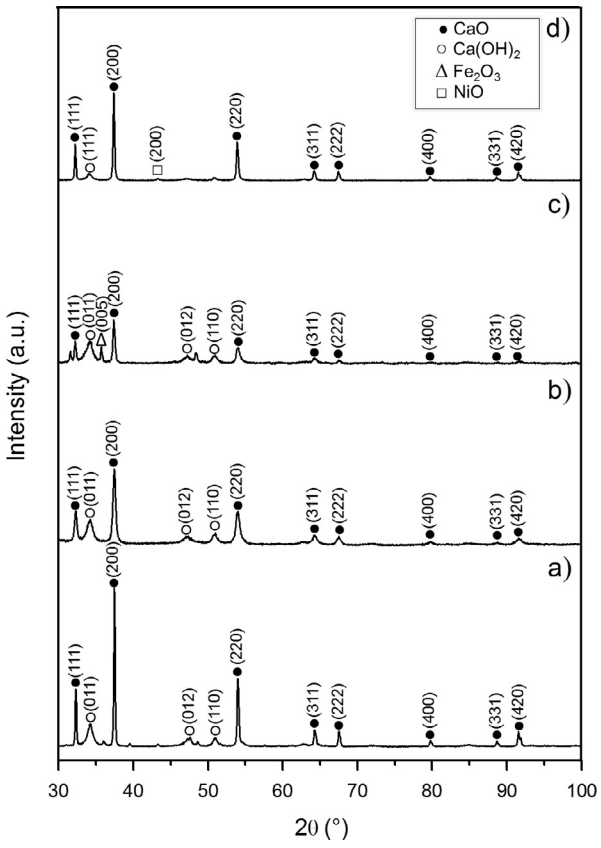

Figure 2 X-ray diffraction patterns of the CaO-based adsorbents prepared: (a) CaO-CS sample, (b) CaO-BM sample, (c) CaO-Fe sample, and (d) CaO-Ni sample.

3.1. XRD patterns

Fig. 2 shows XRD patterns of CaO-based adsorbents prepared by solution combustion and treated using a high-energy ball-milling process. In this figure, all the prepared samples show sharp and well-defined peaks that correspond to pure crystalline calcium oxide indexing to the crystalline cubic lime (JCPDS No. 01-082-1690) file, showing all the corresponding reflections: (111), (200), (220), (311), (222), (400), (331), and (420). Additionally, other small crystalline structures appeared as traces on the $Ca(OH)_2$ (JCPDS No. 01-072-0156) file, with reflections in (011), (012), (110); the Fe_2O_3 (JCPDS No. 00-033-0664) file, with reflections in (110); the FeO(OH) (JCPDS No. 00-046-1315) file, with reflections in (005); and the NiO (JCPDS No. 00-047-1049) file, with reflections in (200), per CaO material preparation. To be sure that no organic radicals remained due to urea combustion, infrared experiments were performed using a Nicolet 550 spectrometer, which mixed the samples with KBr conventionally. The infrared spectra (figure not shown) did not show any band attributable to organic urea residues. Therefore, it was inferred that a complete fuel-to-oxidizer reaction occurred.

All produced CaO-based adsorbents were nanocrystalline in nature, and their differences in structure mainly were due to the preparation method. This shows that solution combustion and ball-milling processes produce nanocrystalline materials with different crystallinity. When CaO is prepared by combustion solution method at 800 °C for 5 min, the CaO-CS sample (Fig. 2a) showed high crystalline lime structure with high uniformity and intensity peaks, with the presence of Ca $(OH)_2$ as a trace residue attributed to the absorbed moisture present in the atmosphere due to the hygroscopic nature of CaO. This $Ca(OH)_2$ structure fraction was observed for all obtained CaO-based powders due to the same conditions under which the fractions occurred. When the CaO-CS sample was treated by high-energy ball-milling over 2.5 h, the CaO crystalline structure changed (Fig. 2b), showing a remarkable decrease in CaO peak intensity and widening, indicating that a significant reduction in crystallinity had occurred by high-energy ball-milling; this behavior can be due to the fragmentation and fracture of starting CaO particles, together with the amorphization degree caused by the ball-milling process. As expected, the CaO crystallinity was affected notably by the high-energy ball-milling treatment, although a calcium oxide nanocrystalline single phase was attained over 2.5 h of ball milling. As the ball-milling time was increased to 10 h for this sample, further reduction in crystallinity was observed through XRD analysis (figure not shown). However, regarding the textural properties of these obtained CaO powders, the BET specific surface area of the CaO sample that underwent ball-milling over 2.5 h decreased from 50.73 m^2/g to 3.87 m^2/g after being treated by ball-milling over 10 h. Furthermore, no significant refinement in particle sizes was observed, because fine, discrete particles are not clearly visible in these samples, and particle agglomerates were observed. Therefore, a reduction in specific surface area for the CaO sample milled over 10 h was generated, implying a smaller amount of active surface sites available for CO_2 adsorption. It is well known that the specific surface area of an adsorbent affects its adsorption behavior. Greater specific surface area leads to greater adsorption of the adsorbing gas on the solid. Consequently, a dramatic reduction in the specific surface area makes the solid unsuitable for enhancing the capture of CO_2 in this CaO ball-milled over 10 h material. According to Suwanboon et al. (2011), the XRD diffraction peaks can reduce and disappear when the materials are milled over long periods, due to the stress induced by the structural defects created during the ball-milling process. The reduction in this sample's crystallinity can have a great influence on the CO_2 capture efficiency, along with other factors such as particle size and morphology, which also will be determinants. Then, the CaO base adsorbent formed during ball milling at 2.5 h was used for further characterization and CO_2 capture. Many studies have shown the effects milling has on the crystal structure of solids (Reid et al., 2008). The structure can be damaged by milling due to the increase in coherent crystal length, which can be explained as a function of the promoted mobility of atoms in the solid. According to Valverde et al. (2014), when CaO is subjected to multiple carbonation/calcination cycles, ball milling has a great influence on the deduction of crystallization, which favors diffusion and serves to promote recarbonation. This observation can be in accordance with the mechanism of carbonation of CaO for CO_2 diffusion through the $CaCO_3$ product layer formed by carbonation of imperfect CaO crystals. On the other hand, XRD patterns of the CaO-Fe adsorbent prepared by high-energy ball milling over 10 h (Fig. 2c) and the CaO-Ni adsorbent prepared by high-energy ball milling over 5 h (Fig. 2d) showed traces of Fe_2O_3, FeO(OH), and NiO structures, with main peaks at 33.2° and 35.6° in 2θ for

CaO-Fe and at 43.3° in 2θ for CaO-Ni, respectively. These samples produced Fe and Ni inter-diffusion in the CaO matrix, facilitated by the ball-milling process. These results indicate that the metallic elements diffuse into CaO, causing the formation of Fe_2O_3, FeO(OH), and NiO structures, respectively, induced by thermal activation generated by the high-energy ball-milling process (Shiri et al., 2014).

For crystallite sizes, the peak-width analysis from the prime reflections with considerable intensities such as (111), (200), and (220) of CaO-based adsorbents using Scherrer's equation revealed a crystallite size of 45.30 nm for the CaO-CS sample, 18.61 nm for the CaO-BM sample, 39.03 nm for the CaO-Fe sample, and 27.34 nm for the CaO-Ni sample, respectively. The CaO-CS sample exhibited the largest crystalline crystallite size (45.30 nm) of all the CaO phases. This was attributed to the high flame temperatures during the fast combustion process caused by the reaction between $Ca(NO_3)_2{\cdot}4H_2O$ and urea. However, the fast combustion did not affect the position of the crystals' reflexions, as reported in the specialized literature. The crystallite size of the CaO sample obtained through the combustion solution and treated by ball milling for 2.5 h, revealed a markedly decreased crystallite size of 18.61 nm, due to repeated powder welding and fracturing caused by the steel balls used in the ball-milling process. This is in line with Granados-Correa et al.'s (2008) previous observations. This implies that the particle size becomes smaller during milling without the formation of a new phase. According to Biasin et al. (2015), when a CaO sample has smaller crystallite sizes, it shows a larger length of crystallite limits per unit of specific surface area and consequently, a larger active specific surface area for the occurring $CaO\text{-}CO_2$ reaction during the CO_2 capture process. On the other hand, the observed reduction in crystallite size of the CaO-Fe and CaO-Ni nanocomposite samples could be attributed to the protective covering that the respective metals provided to CaO.

3.2. N_2 physisorption measurements

The main surface characteristics of the four selected CaO-based adsorbents prepared by solution combustion and high-energy ball milling are shown in Table 1. As can be seen, the specific surface area of the CaO-CS sample is large (24.32 m^2/g). This could be caused by cavities created on the surface associated with the solution-combustion reaction related to gas emissions during combustion and bubble explosion forming craters and cavities, which can be observed in the SEM micrographs (Fig. 5a). Such morphologies reveal the presence of vapors that are liberated when the sample is viscous (Granados-Correa et al., 2008). However, the BET specific surface area of CaO increased twofold, from 24.32 m^2/g to 50.73 m^2/g after high-energy ball milling of CaO for 2.5 h. The increased specific surface area is the result of fracture creation and average particle-size reduction caused by the ball-milling process (Bonifacio-Martínez et al., 2009). It is well known that the high-energy ball-milling process generates high temperatures, which cause atomic inter-diffusion in the raw structure that facilitates a homogeneous distribution in a short time (Kostic et al., 1997). The milling treatment led to an increase in the specific surface area due to those small particles. Generally, an inverse proportionality between BET specific surface area and particle size is assumed; therefore, the ball-milling process in this case is essential to obtain large specific surface areas. The CaO-Fe and CaO-Ni samples resulted in a specific surface reduction of 28.489 m^2/g and 10.209 m^2/g, respectively. This phenomenon can be associated with the mechano-chemical process, leading to sample compaction/shrinkage, and is accompanied by decreases in specific surface areas. In addition, these CaO-Fe and CaO-Ni nanocomposite results corroborate the negative effect of adding some transition metals to the CaO structure. For example, Ravikovitch and Neimark (2002) studied a new classification of physical mechanisms of adsorption hysteresis in ink-bottle-type pores and proved that a specific surface area reduction can be attributed to the blocked pores due to the deposition of the dopant particle into the material support structure. However, the CaO-CS and CaO-BM samples exhibited larger

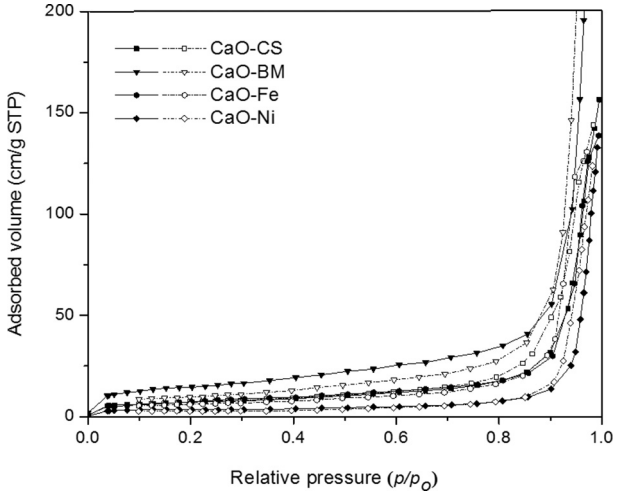

Figure 3 N_2 adsorption-desorption isotherms of CaO-based adsorbents: CaO-CS, CaO-BM, CaO-Fe, and CaO-Ni samples at 77 K, previously outgassed at 250 °C over 3 h.

Table 1 Textural properties of CaO-based adsorbents obtained by N_2 physisorption measurements, samples degassed at 300 °C for 3 h.

Sample	N_2 physisorption measurements			Pore size distribution (BJH)		
	A_{BET} (m^2/g)	V_{TOT} (cm^3/g)	D_p (nm)	$A_{BET\ mesopore}$ (m^2/g)	$V_{TOT\ mesopore}$ (cm^3/g)	$V_{mesopore}$ fraction (%)
CaO-CS	24.3	0.229	33.06	25.271	0.227	99.08
CaO-BM	50.7	0.548	38.48	52.124	0.543	99.01
CaO-Fe	28.4	0.211	44.92	28.957	0.210	99.57
CaO-Ni	10.2	0.199	44.92	8.789	0.196	98.59

Please cite this article in press as: Granados-Pichardo, A. et al., New CaO-based adsorbents prepared by solution combustion and high-energy ball-milling processes for CO_2 adsorption: Textural and structural influences2 adsorption –>. Arabian Journal of Chemistry (2017), http://dx.doi.org/10.1016/j.arabjc.2017.03.005

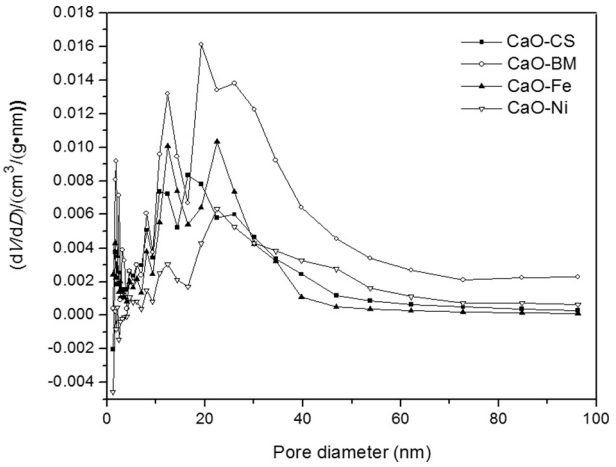

Figure 4 Pore-size distribution of CaO-based adsorbents obtained by BJH method for CaO-CS, CaO-BM, CaO-Fe, and CaO-Ni samples.

specific surface areas, which will be responsible for their relatively better CO_2 adsorption performance. The high concordance between the specific surface area and adsorption values indicates that a greater specific surface area could provide more contact areas to which the adsorbent particles can be exposed to CO_2, promoting the reaction of CaO with CO_2 (Hu et al., 2016). On the other hand, materials with nanometric pore diameters greatly increase the adsorption diffusion path and the entrapment of CO_2 in the adsorbent structure while improving mass transfer during the adsorption/desorption process (Fennell et al., 2007). Thus, the specific surface area, the pore-size distributions, and the morphology of adsorbents are some of the parameters that cause reactivity and adsorption effects, which determine their CO_2 capture application. Therefore, the main differences between the not-ball-milled CaO and the ball-milled CaO samples must be textural: Specific surface area and surface CO_2 adsorption properties must be different.

Adsorption isotherm curves for studied CaO-based adsorbents are presented in Fig. 3. When the amount of N_2 adsorbed was plotted against the relative pressure, all CaO-based samples resulted in BET type-IV isotherms, which indicates that mesoporous solids were generated. In addition, type H1 hysteresis loops were shown in the N_2 adsorption-desorption isotherm measurements, which indicates that they were produced by either slit-shaped pores or particle agglomeration during sample preparation (Mangal et al., 2013).

CaO-based adsorbents' pore-size distributions determined by the BJH method are shown in Fig. 4. As can be seen, the average pore diameter of CaO prepared by the combustion solution sample without ball milling was 33.06 nm. However, the average pore diameter of the CaO sample prepared by solution combustion increased from 33.06 to 38.48 nm after the ball-milling process over 2.5 h. This phenomenon usually is described as a mechano/chemical process, leading to sample compaction/shrinkage, which is accompanied by a decrease in pore size. According to Bai et al. (2011), the fuel-to-oxidant ratio had a significant influence on the pore-size distribution of the combustion-synthesized powders, because the control of the strong exothermal urea combustion is essential to form porous materials. In this context, a molar ratio of chemical precursor fuel to oxidizer (2:1) was used in agreement with fuel-oxidizer mixtures and their elemental stoichiometric coefficient (φ_e), which predicts the fuel richness or leanness of the composition applicable to the multicomponent system in the field of propellants and explosives. The combustion reaction is classified as *rich in fuel* based on the total oxidizing and reducing valences of the oxidizer and the fuel maintaining the oxidized/fuel ratio's unity (Mimani and Patil, 2001; Jain

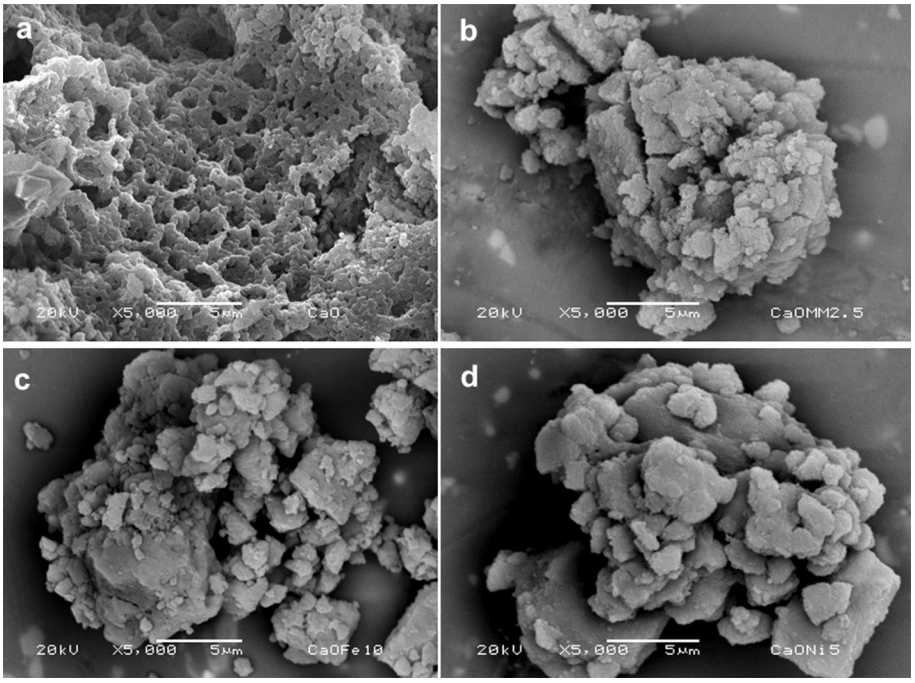

Figure 5 SEM micrographs of (a) CaO-CS sample, (b) CaO-BM sample, (c) CaO-Fe sample, and (d) CaO-Ni sample.

et al., 1981; Patil et al., 1997). Combustion reaction is related to the energetics of such mixtures to form a pore-extended structure of solids, because this combustion technique requires significant amounts of energy. In general, CaO-based adsorbents have irregular pore-size distributions, showing a bimodal pore-size distribution in the small mesopore range (< 15 nm) and in the large mesopore range (< 30 nm). In this context, the calculated mesopore fraction shown in Table 1 indicated that in all cases, more than 98% were mesoporous materials (D_p < 50 nm) in concordance with the International Union of Pure and Applied Chemistry (IUPAQ) pore classification.

Fennell et al. (2007) established that a narrow pore-size distribution is expected to play an important role based on studies on carbonation at high temperatures for calcium looping. On the other hand, the small pores, especially those located near the sorbents' particle surface, are clogged, and this closure of pores close to the particle surface prevents CO_2 diffusion toward the partially reacted core. Thus, obtaining mesopores could play an important role in CO_2 capture.

3.3. SEM analysis

The surface morphology and structural features of CaO-based powder from combustion solution and ball-milling processes are compared in Fig. 5. CaO combustion-solution sample morphology (Fig. 5a) represents a characteristic voluminous and fluffy combustion product with a coral-shaped morphology and a rough and porous structure with some cavities, showing an uniform and compact distribution of the particles. This structure is obtained because of associated formations of materials with vigorous evolutions of the large volume of gases generated during the combustion reaction. The images obtained from the CaO ball-milled sample over 2.5 h and their respective CaO-Fe and CaO-Ni composites (Fig. 5b–d) show a dominant fragmentation pattern and surface irregularities with certain well-squared, crystallized nanoparticles of agglomerated CaO, which can be ascribed to the high pressure exerted by the milling balls on the materials.

The CaO-Fe sample (Fig. 5c) showed an agglomeration of small, square particles that can be attributed to the Fe_2O_3 formation. The quantity of these square particles is low due the low concentration of Fe used in the mixture. The CaO-Ni sample (Fig. 5d) showed agglomerated particles. However, this material exhibited smaller-sized particles compared to the other samples. Baird et al. (1992) demonstrated that when they doped ZnO with transition-metal oxides, smaller particles of ZnO were formed. This could be attributed to inter-diffusion metal atoms in the ZnO matrix. The results above were consistent with the XRD patterns and the crystallite size calculated from XRD peak broadening using the Scherrer equation. In general, irregular pore structures created by the fusion of agglomerates are seen in the SEM micrographs. However, BET specific surface area and total pore volume for CaO-CS, CaO-Fe, and CaO-Ni provided in Table 1 confirm the difference among the three materials. EDS analysis was carried out to study the elemental composition of these nanocrystals. The analysis showed the presence of calcium and oxygen in all CaO-based adsorbents. In the CaO-Fe and CaO-Ni samples, small quantities of the dopant metals, Fe and Ni, respectively, appeared as less than 3% of the total weight. Finally, the doped CaO-based samples confirm the good distribution between Ca and the metals, indicating the suitability of the synthesis method for uniform dispersion of the metals in the solid CaO particles.

3.4. CO_2 capture performance-capacity of adsorbents

The four best CaO-based adsorbents chosen by their most significant structural and textural properties were tested in terms of CO_2 adsorption capacity. First, the saturation time was established using an arbitrary CaO-BM sample. Then, the CO_2 uptake increased rapidly in the first minute and reached saturation 15 min after contacting the phases in the solid/gas system. This clearly indicates a fast reaction stage due to the fast reaction of CO_2 on the outer surface of the CaO nanoparticle to form the $CaCO_3$ layer covering the CaO core. This reaction continues through the structure fractures, until the $CaCO_3$ layer increases the diffusion resistance of CO_2 to react with the CaO core and thus decreases the reaction rate. However, after the relatively fast initial reaction, a slower reaction stage controlled by diffusion into the pores or in the product layer takes place, resulting in a slower reaction rate. This is assumed to occur because the carbonation reaction in the micropores is hindered by the limited space that restricts the growth of $CaCO_3$ (Alvarez and Abanades, 2005). Therefore, all studies were conducted at 25 °C, 1 atm, and 15 min of saturation time. The CO_2 test results showed that the CaO-BM sample exhibited the best CO_2 adsorption capacity of 9.31 mmol/g, compared to the CaO-CS sample (6.35 mmol/g), CaO-Fe sample (3.47 mmol/g), and CaO-Ni sample (4.20 mmol/g). The CO_2 adsorption performance differences between the CaO-BM and CaO-CS samples can be ascribed to the smaller crystal-grain size and fractures created by the milling of the CaO-BM, which created a larger exposed specific surface area, which was beneficial to the interaction between CaO and CO_2, producing a larger and thinner layer of $CaCO_3$, resulting in an easier diffusion of CO_2. The high CO_2 adsorption capacity (9.311 mmol/g) of the CaO-BM sample could be attributed to the elimination of the external mass transfer limitations that affect CaO carbonation. This occurs

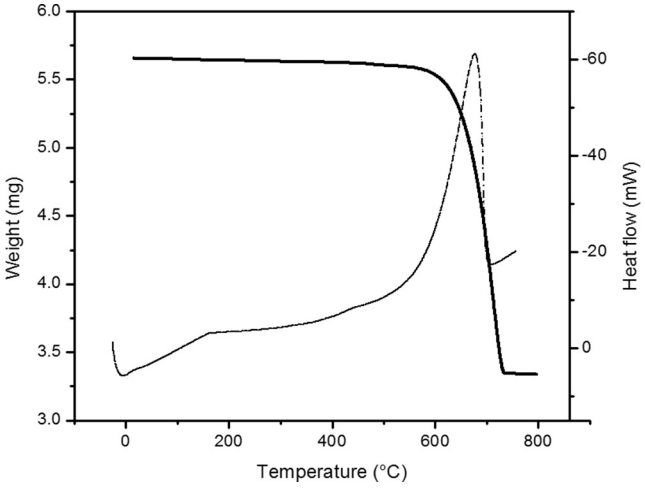

Figure 6 TGA-DSC of CaO-BM sample after CO_2 adsorption at 25 °C and 1 atm.

because of the high gas velocity and CO_2 atmosphere around the CaO-based adsorbents' particles, which support the high CO_2 intake rate attributed to the chemical reaction on the surface. A two-step CO_2 adsorption process takes place, according to the literature (Li et al., 2012). For the first step, it is proposed that the CO_2 adsorption occurred at the solid surface only (Step 1: $CaO + CO_2 \rightarrow CaCO_3$). Thus, the second step is related to CO_2 diffusion into the CaO particles, implying a slow diffusion of CO_2 below the surface but relatively fast adsorption of CO_2 onto the CaO surface, since $CaCO_3$ generated at the surface layers was not sintered by thermal activity because the adsorption temperature (25 °C) was lower than the Tammann temperature (533 °C); therefore, CO_2 adsorption on the surface continued (Phromprasit et al., 2016). Previous results (Rashidi et al., 2013), have showed that for CO_2 capture with CaO-based adsorbents, pores with a diameter narrower than 150 nm are the dominant contribution to the carbonatation reaction; these pores have a high surface area and reasonable pore volume that can accommodate the bulky product, $CaCO_3$. Pores larger than 150 nm are expected to play a lesser role. On the other hand, the CaO-Fe and CaO-Ni samples presented a smaller CO_2 sorption capacity due to Fe and Ni obstructions in the pathway of the active CaO sites. We observed that the CO_2 adsorption behavior of the CaO-based adsorbents was affected by their crystallite sizes, specific surface areas, pore volumes, and pore-size distribution. For CO_2 adsorption, the specific surface area works as a chemical adsorption site for CO_2 and carbonate formation through the carbonation reaction described previously. The pore worked as the diffusion path, and in terms of pore volume, the diffusion resistance was the key factor in kinetic adsorption, because CO_2 adsorption increases when total pore volumes increase and larger pore volumes experienced less diffusion resistance, as stated by Lee et al. (2015a, 2015b).

As shown in Fig. 6, the TGA-DSC of the CaO-BM sample involved measuring the thermal variation associated with the physical and chemical transformations (e.g., dehydration and decomposition) that occurred during the heating of the CaO-BM sample. Typical thermal curves obtained by DSC analysis showed two distinct stages of weight losses: The first stage, at a temperature lower than 680 °C, attributed to the adsorbed water molecules, and the second stage, between 680 and 750 °C, corresponded to the molecular weight of CO_2, implying that $CaCO_3$ was being decarbonized to CaO, until a complete CaO regeneration at 850 °C.

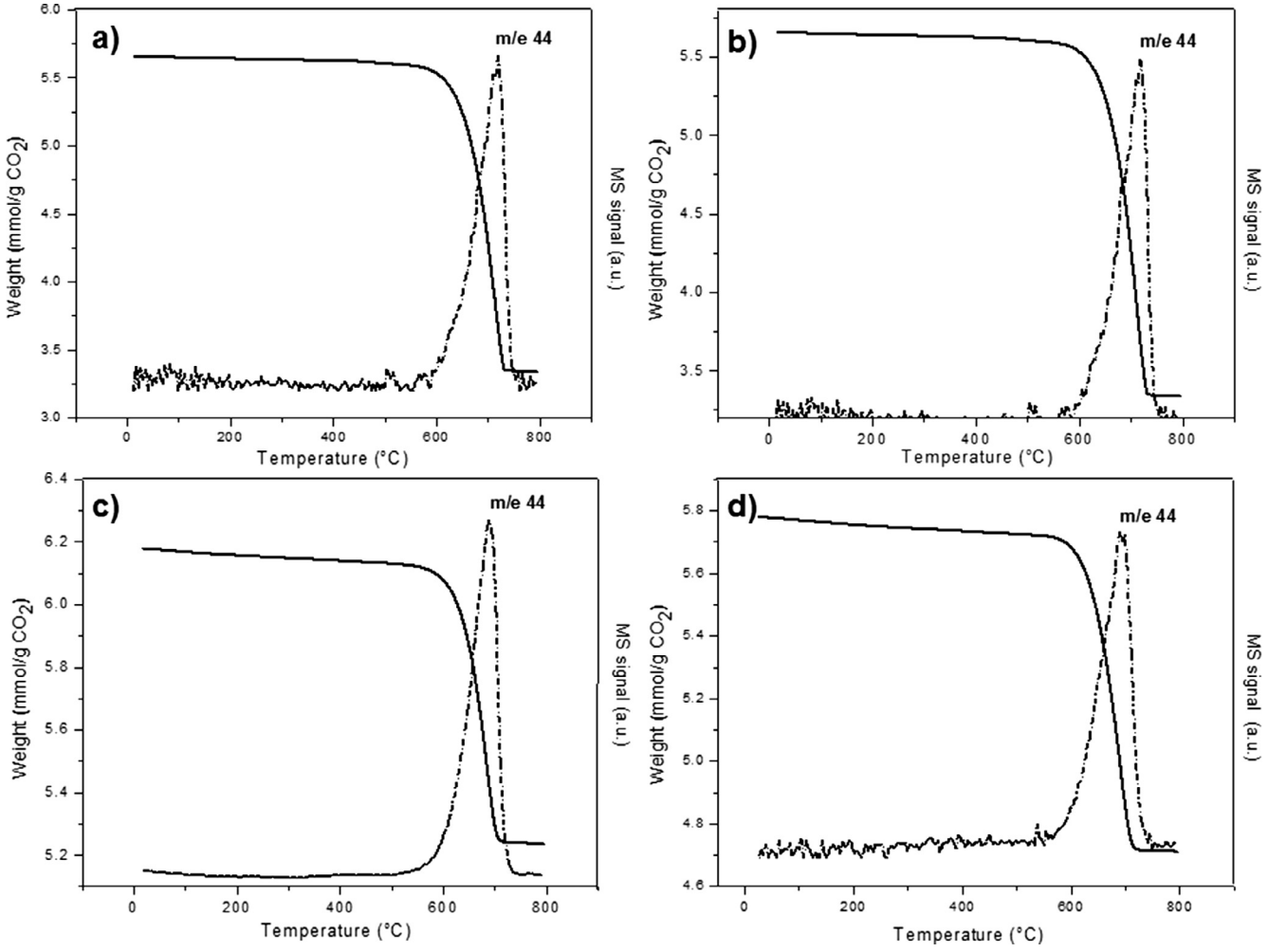

Figure 7 TGA-MS for relative molecular mass 44 (carbon dioxide) as a function of temperature of the CaO-based adsorbents obtained by (a) CaO-CS, (b) CaO-BM, (c) CaO-Fe, and (d) CaO-Ni.

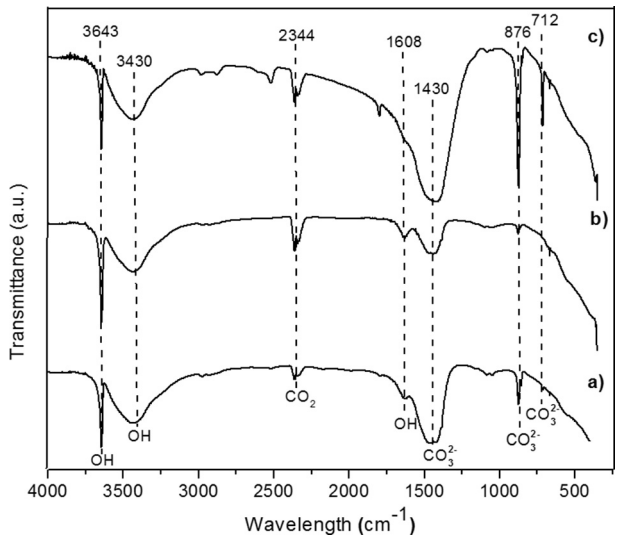

Figure 8 Representative FTIR transmittance spectra from (a) CaO-BM sample, (b) CaO-BM degassed sample, and (c) CaO-BM after CO_2 adsorption process at 25 °C and 1 atm.

Fig. 7 shows the thermogravimetric analysis linked to mass spectrometry (TGA-MS) of the four selected CaO-based adsorbents after CO_2 adsorption at 25 °C and 1 atm over 15 min of equilibrium time, with the purpose of proving the quantity of CO_2 adsorbed during the carbonation process. Experimental setup by using pure CO_2 gas in a stainless reactor Parr 4592 of 50 mL capacity coupled with a temperature-controlled system was carried out at different atmospheres and temperatures. Then, samples were taken from the system and analyzed in a TGA thermogravimetric analyzer. Carbonatations were calculated from the calcination profiles of TGA-MS analysis from 20 °C to 850 °C. The TGA-MS spectrum, showed the following decreases in weight percentage: 27.06 weight percentage for the CaO-CS sample, 40.28 weight percentage for the CaO-BM sample, 14.46 weight percentage for the CaO-Fe sample, and 17.48 weight percentage for the CaO-Ni sample, respectively. In all cases, an endothermic peak related to the theoretical losses in weight percentage of CO_2 that is released during the calcination of $CaCO_3$ was observed and confirmed by the mass spectrometry analysis (Faatz et al., 2004). In addition, the Fe and Ni added to the CaO apparently did not affect the CaO de-carbonation process.

Different analytical methods, such as FTIR, XRD and XPS, were carried out to investigate the carbonatation reaction through a CO_2 chemisorption mechanism, on the surface condition of the CaO adsorbent prepared by solution combustion at 800 °C over 5 min and treated by high-energy ball-milling over 2.5 h (CaO-BM). In Fig. 8, three characteristics of FTIR transmittance spectra were obtained using an IR Nicolette 550 spectrometer with a conventional method KBr disk from a CaO sample prepared by solution combustion at 800 °C over 5 min and treated by high-energy ball milling over 2.5 h (CaO-BM) without any pretreatment (Fig. 8a), from a CaO-BM sample degassed at 300 °C over 30 min (Fig. 8b), and from a CaO-BM sample after CO_2 adsorption process at 25 °C and 1 atmosphere (Fig. 8c). In all, the FTIR spectra bands at 1430, 876, and 712 cm^{-1} are attributed to the CO_3 group of calcite, which are consistent with other results (Smith, 1999). In addition, the strong sharp band, which is characteristic of the O-H stretching vibration in $Ca(OH)_2$, occurs at 3643, 3430, and 1608 cm^{-1} in the spectra samples that contained hydroxide. In the degassed sample (Fig. 6b), the broad band around 1400–1500 cm^{-1}, as well as a weak band at 876 cm^{-1}, indicates the rapid formation of the carbonate from the hydroxide (Legodi et al., 2001). The small band centered at 1784 cm^{-1} only appeared in the sample with CO_2, which may be assigned to monodentate carbonate (Philipp and Fujimoto, 1992). The band at 2314 cm^{-1} in all spectra indicates the existence of physisorbed carbon dioxide (Ding et al., 2015). Then, based on these results, it is further demonstrated that the adsorption mechanism of the CaO-BM2.5 h sample was mainly relying on chemisorption accompanying with a very small fraction of physisorption.

On the other hand, for the CaO-BM sample with CO_2, a typical XRD characterization was carried out to confirm the $CaCO_3$ formation. The XRD result showed principal peaks that corresponded to the calcite structure (JCPDS No. 05-0586) file and cubic calcium oxide (JCPDS No. 37-1497) file, indicating less intensity. The X-ray diffraction pattern of CaO-BM after CO_2 adsorption (Fig. 9) showed a major peak at $2\theta = 39.4°$, indicating that calcite ($CaCO_3$) is a major phase of the sample. The CaO phase with 2θ values of 32.3°, 37.4°, 53.9°, 64.2°, 67.375°, 79.665°, 88.525°, and 91.459° was found in a smaller amount due to partial carbonation, which CaO experienced during CO_2 contact, which demonstrated the carbonate's presence.

For surface analysis, Fig. 10 shows the high-resolution XPS spectra of the three major elements on the CaO-BM sample after CO_2 adsorption, including carbon, oxygen, and calcium elements showing high levels of carbon due to calcium carbonate surfaces with high surface energy BE values (in eV) and the atomic concentration (in percentages) of the elements of this sample. The C1s signal shows the contributions assigned to carbonate in 289.8 eV and 290.8 eV (Fig. 10a). The O1s signal appears at 531.7 and 531.0 eV, corresponding mainly to calcium carbonate (Fig. 10b). On the other hand, only one peak at 347.3 eV in the Ca2p spectra was identified as a CaO remnant on the surface (Fig. 10c). Apparently, it was shown that 31.71% of the carbonate was deposited on the CaO surface

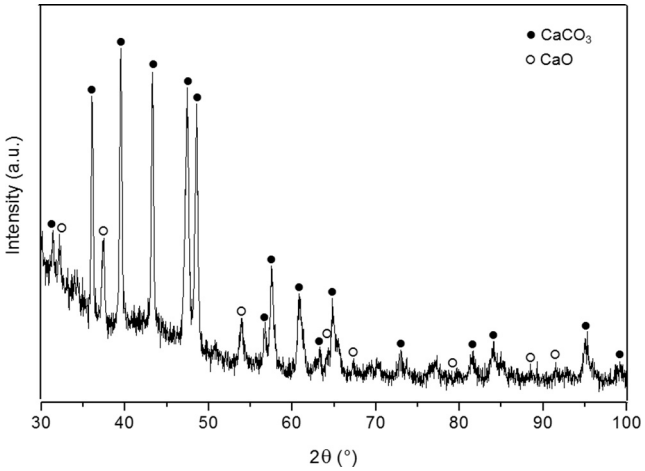

Figure 9 X-ray diffraction pattern of the CaO-BM sample after CO_2 adsorption process at 25 °C and 1 atm.

Please cite this article in press as: Granados-Pichardo, A. et al., New CaO-based adsorbents prepared by solution combustion and high-energy ball-milling processes for CO_2 adsorption: Textural and structural influences2 adsorption –>. Arabian Journal of Chemistry (2017), http://dx.doi.org/10.1016/j.arabjc.2017.03.005

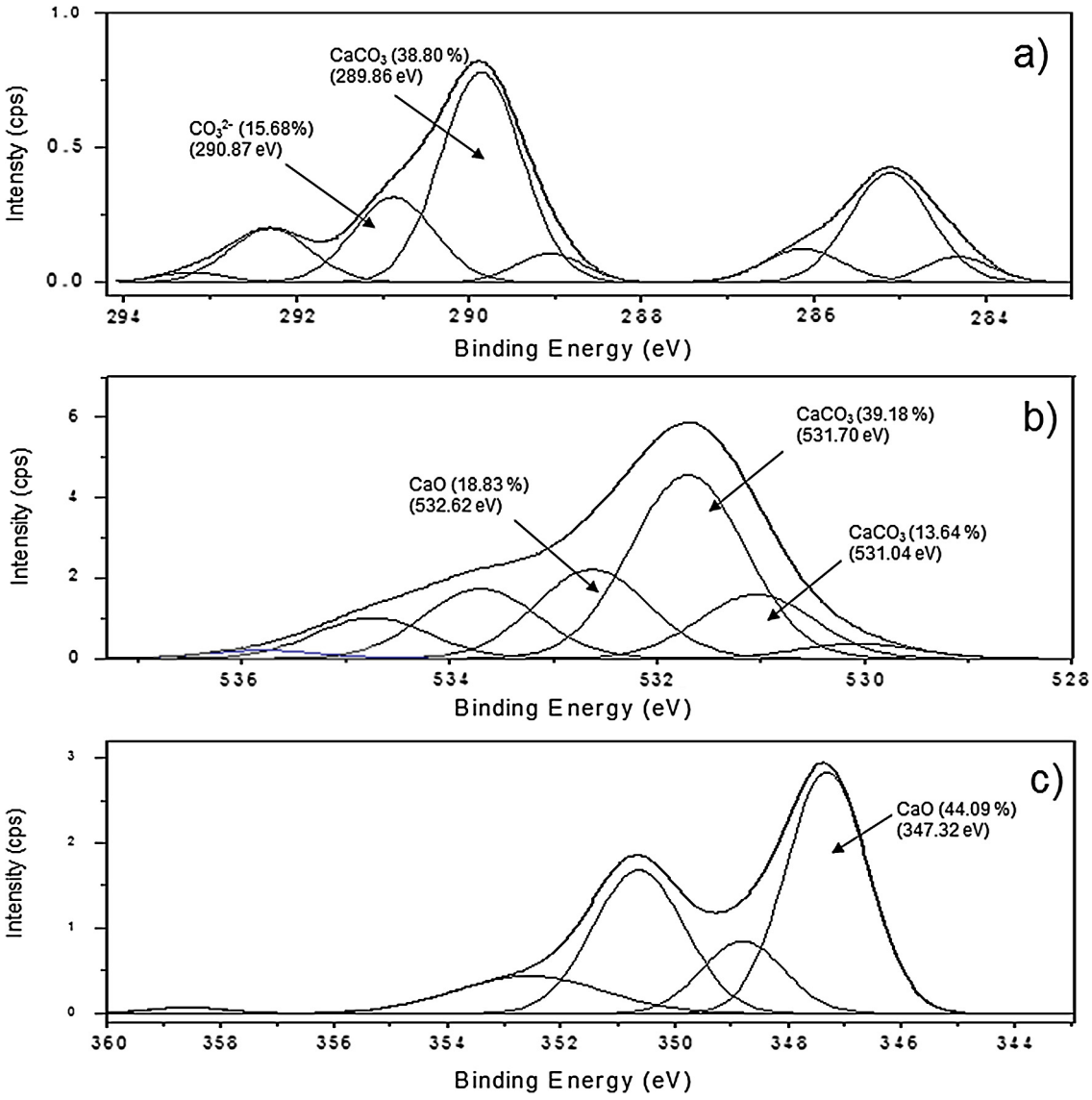

Figure 10 XPS peaks of CaO after CO_2 adsorption process, (a) C1s, (b) O1s, and (c) Ca 2p.

after 15 min of CO_2 exposure. About 18.31% of the Ca surface was free from carbonate deposition, and the other 49.97% was divided between $CaCO_3$ and CaO. This carbonate occurred by chemical reaction between the CaO surface and high concentrations of CO_2 to form a weak and strong chemical bonding on the metal surface. In general, the yield of formed $CaCO_3$ shows that this material could adsorb CO_2 very well at room temperature and pressure.

3.5. Multi-cycle performance of CaO-BM adsorbent

Good adsorbent stability is necessary for CO_2 adsorbent technological applications (e.g., in the CO_2 capture of CaO-based adsorbents in looping cycles). The CaO-BM sample was chosen to test this parameter. As can be seen in Fig. 11 the increase in the number of cycles does not have a significant impact on the CO_2 adsorption capacity. The results imply that after five cycles, the modified adsorbent is stable, with CO_2 capture capacities of 9.23 mmol/g for the first cycle and 9.07 mmol/g for the fifth cycle, representing a 1.7% decrease. The adsorption runs were carried out using high purity CO_2 (99.9%) gas at 25 °C under atmospheric pressure while the regeneration was carried out under helium flow from 20 °C to 850 °C. The decrease in the conversion through reaction cycles was caused by pore blockage and collapse, which induced greater CO_2 diffusion resistance because of the lower specific surface area and small pores. According to the literature, when CaO is calcined at 850 °C, sintering reduces the specific surface area and causes the pores to shrink. Thus, the limiting factor for further reactions is not pore blockage but rather the inhibition of CO_2 ion diffusion through the $CaCO_3$ product layer (Li et al., 2012). Our results indicated that the studied material is stable after five cycles of CO_2 capture. The original CO_2 adsorption capacity of CaO-BM sample was 9.31 mmol/g, and during the 1st cycle of 9.23 mmol/g, these cyclic performance data indicate that CaO-BM sample presented a low deterioration of their CO_2 capturing performance. Comparatively, CO_2 adsorption performance carried out at 25 °C and 1 atm of only their 1st

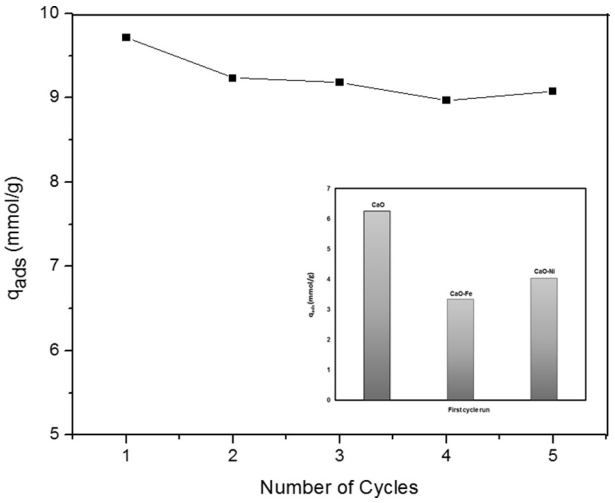

Figure 11 CO_2 adsorption/desorption cycles of modified CaO-BM sample at 25 °C and 1 atm with 15 min of saturation time. The inset image is the 1st cycle adsorption of CaO-CS sample, CaO-Fe sample, and CaO-Ni sample at 25 °C and 1 atm.

cycle adsorption on the other three adsorbents studied in the present work were inserted into Fig. 11. As was observed, their 1st recycle runs indicated that the CaO-sample decreased from 6.35 mmol/g to 6.255 mmol/g of CO_2 adsorption capacity, the CaO-Fe sample decreased from 3.47 mmol/g to 3.34 mmol/g, and the CaO-Ni sample decreased from 4.20 mmol/g to 4.04 mmol/g respectively. Therefore, it can be concluded that these studied materials are also stable for CO_2 capture. Previous reports over CaO multicyclic loss of adsorbent activity during carbonatation/calcination cycles are consistent with our results and showed similar stability with an increasing number of cycles (Kavosh et al., 2015; Kazi et al., 2014; Sun et al., 2016; Valverde et al., 2014; Wang et al., 2014).

4. Conclusions

The results of this work highlight the advantages of using ball-milling process during the preparation of CaO-based adsorbents in a short reaction time. Using this process, it was possible to prepare a promising and stable CaO-based adsorbent for efficient CO_2 capture due to its improved structural and textural properties. The results show that the ball-milling CaO-based adsorbent, of nanocrystalline and mesopore structure, allowed high $CaCO_3$ conversion from CaO when the sample was subjected to a CO_2 flow at 25 °C and 1 atm by CO_2 intra-diffusion over the CaO adsorbent surface. The observed beneficial effect of high conversion from CaO to $CaCO_3$ was attributed to nano-adsorbent's fluffy structure, significantly BET specific surface area, and large pore volume. The CO_2 adsorption process in the nanosized CaO-based adsorbent obtained by solution combustion and treated by ball-milling during 2.5 h (CaO-BM) was mainly by chemisorption with an exothermic reaction forming $CaCO_3$, accompanying with a very small fraction of physisorption which was corroborated by FTIR, XRD and XPS studies. The experimental results revealed that the CO_2 adsorption behavior on CaO-BM adsorbent is significant and a feasible procedure can be deployed for the post-combustion CO_2 capture, and that the ball-milling process plays a vital role to promote their CO_2 capture at ambient temperature and pressure, which was showed by TGA-MS results. This is a desirable feature for the operation of a CO_2 capture system as an important design consideration to minimize the energy expenditure. For future tests, the effect of higher temperature on the performance of this system over CO_2 adsorption should be investigated.

Acknowledgments

The authors acknowledge the National Institute of Nuclear Research (ININ) and the Department of Chemistry for their support in conducting this research through the project ININ CB-406 (Stages I-III) and UAEMex (CONACYT project 388496). Additionally, the authors thank CONACYT for the scholarship provided during the project. We also thank Dr. Rafael Basurto-Sánchez for technical help in XPS analysis.

References

Alexeeva, V., Anger, N., 2015. Mitigat. Adapt. Strat. Glob. Change 21, 1–26.
Alvarez, D., Abanades, J.C., 2005. Ind. Eng. Chem. 44, 5608–5615.
Ammendola, P., Raganati, F., Chirone, R., 2015. Particuology 134, 494–501.
Aruna, S.T., Mukasian, A.S., 2008. Curr. Opin. Solid State Mater. Sci. 12, 44–50.
Bai, J., Liu, J., Li, C., Li, G., Du, Q., 2011. Adv. Powder Technol. 22, 72–76.
Baird, T., Denny, P.J., Hoyle, R., McMonagle, F., Stirling, D., Tweedy, J., 1992. J. Chem. Soc. Faraday Trans. 88, 3375–3382.
Barret, E.P., Joyner, L.G., Halenda, P.P., 1951. J. Am. Chem. Soc. 73, 373–380.
Belmabkhout, Y., Guillerm, V., Eddaoudi, M., 2016. Chem. Eng. J. 296, 386–397.
Ben-Mansour, A.R., Habib, M.A., Bamidele, O.E., Basha, M., Oasem, N.A.A., Peedikakkal, A., Ali, M., 2016. Appl. Energy 161, 225–255.
Bhatt, P.M., Belmabkhout, Y., Cadiau, A., Adil, K., Shekhah, O., Shkurenko, A., 2016. J. Am. Chem. Soc. 138, 9301–9307.
Bhatta, L.K.G., Subramanyam, S., Chengala, M.D., Olivera, S., Venkatesh, K., 2015. J. Clean Prod. 103, 171–196.
Biasin, A., Segre, C.U., Salviulo, G., Zorzi, F., 2015. Chem. Eng. Sci. 127, 13–24.
Bonifacio-Martínez, J., Serrano-Gómez, J., López-Reyes, del Carmen, Ma., Granados-Correa, F., 2009. Clay Miner. 44, 311–317.
Datta, S.J., Khumnoon, C., Lee, Z.H., Moon, W.K., Docao, S., Nguyen, T.H., Hwang, I.C., Moon, D., Oleynikov, P., Terasaki, O., Yoon, K.B., 2015. Science 350, 302–306.
Ding, Y., Song, G., Zhu, X., Chen, R., Liao, Q., 2015. RSC Adv. 5, 30929–30935.
Dou, B., Song, Y., Liu, Y., Feng, C., 2010. J. Hazard. Mater. 183, 759–765.
Drage, T.C., Smit, K.M., Arenillas, A., Snape, C.E., 2009. Energy Proc. 1, 875–880.
Duan, Y., Sorescu, D.C., 2010. J. Chem. Phys. 133, 074508–074511.
Faatz, M., Gröhn, F., Wegner, G., 2004. Adv. Mater. 16, 996–1000.
Feng, B., Liu, W., Li, X., An, H., 2006. Energy Fuels 20, 2417–2420.
Fennell, P.S., Pacciani, R., Dennis, J.S., Davidson, J.F., A.N. Hayhurst, A.N., 2007. Energy Fuels 21, 2072–2081.
Feron, P.H.M., 2010. Int. J. Greenh. Gas Control 4, 152–160.
Florin, N., Fennell, P., 2011. Energy Procedia 4, 830–838.
García, S., Gil, M.V., Martín, C.F., Pis, J.J., Rubiera, F., Pevida, C., 2011. Chem. Eng. J. 171, 549–556.
Granados-Correa, F., Bonifacio-Martínez, J., Hernández-Mendoza, H., Bulbulian, S., 2016. J. Air Waste Manage. Assoc. 66, 643–654.
Granados-Correa, F., Bonifacio-Martínez, J., Lara, V.H., Bosch, P., Bulbulian, S., 2008. Appl. Surf. Sci. 254, 4688–4694.
Hakim, L.F., Portman, J.L., Casper, M.D., Weimer, A.W., 2005. Powder Technol. 160, 149–163.

Hennessy, J., 2015. Nature Mater. 14. 857-857.
Hou, C., Liu, Q., Wang, P., Sun, W.Y., 2013. Microporous Mesoporous Mater. 172, 61–66.
Hu, Y., Liu, W., Wang, W., Sun, J., Yang, X., Chen, H., Xu, M., 2016. Chem. Eng. J. 296, 412–419.
Hwang, C., Wu, T., 2004. Mater. Sci. Eng. B 111, 197–206.
Ibarahim, N.A., Osman, N., Ishak, M., Azlan, M., 2015. Adv. Mater. Res. 1108, 67–72.
Jain, S.R., Adiga, K.C., Verneker, V.P., 1981. Flame 40, 71–79.
Janusz, W., Khalameida, S., Sydorchuk, V., Skwarek, E., Zazhigalov, V., Skubiszewska, Z.J., Leboda, R., 2010. Adsorption 16, 333–341.
Kavosh, M., Patchigolla, K., Oakey, J.E., Anthony, E.J., Champagne, S., Hughes, R., 2015. Chem. Eng. Res. Des. 102, 116–123.
Kazi, S.S., Aranda, A., Meyer, J., Mastin, J., 2014. Energy Procedia 63, 2207–2215.
Khomane, R.B., Sharma, B.K., Saha, S., Kulkarni, B.D., 2006. Chem. Eng. Sci. 61, 3415–3418.
Kostic, E., Kiss, S., Boskovic, S., Zec. S., 1997. Powder Technol. 91, 49–54.
Lee, C.H., Hyeon, D.H., Jung, H., Chung, W., Jo, D.H., Shin, D.K., Kim, S.H., 2015a. J. Ind. Eng. Chem. 23, 251–256.
Lee, Z.H., Ishikawa, S., Lee, K.T., Mohamed, A.R., 2015b. J. Energy Chem. 24, 225–231.
Legodi, M.A., De Waal, D., Potgieter, J.H., Potgieter, S.S., 2001. Miner. Eng. 14, 1107–1111.
Li, Z., Fang, F., Tang, X., Cai, N., 2012. Energy Fuels 26, 2473–2482.
Li, Z., Liu, Y., Cai, N., 2014. Fuel 127, 88–93.
Liang, G., Hout, J., Schultz, R., 2001. J. Alloys Compound. 320, 133–139.
Liu, W., Low, N.W., Feng, B., Wang, G., Diniz da Costa, J.C., 2008. Environ. Sci. Technol. 44, 841–847.
Lu, C., Zheng, Y., Xu, Y., Ding, N., Shen, Q., Zheng, C., 2015. Chem. Eng. J. 267, 111–116.
Lu, H., Reddy, E.P., Smirniotis, P.G., 2006. Ind. Eng. Chem. Res. 45, 3944–3949.
Mangal, H., Saxena, A., Rawat, A.S., Kumar, V., Rai, P.K., Datta, M., 2013. Microporous Mesoporous Mater. 168, 247–256.
Manovic, V., Anthony, E.J., 2008. Energy Fuels 22, 1851–1857.
McCarthy, J.J., Leary, O.F., Dokken, N.A., White, K.S.D.J., 2001. Climate Change. Cambridge University Press, UK.
Mimani, T., Patil, K.C., 2001. Mater. Phys. Mech. 4, 134–137.
Pacciani, R., Müller, C.R., Davidson, J.F., Dennis, J.S., Hayhurst, A. N., 2008. J. Chem. Eng. 86, 356–366.
Patil, K.C., Aruna, S.T., Ekambaram, S., 1997. Curr. Opin. Solid State Mater. Sci. 2, 158–165.
Patterson, A.L., 1939. Phys. Rev. 56, 978–982.
Philipp, R., Fujimoto, K., 1992. J. Phys. Chem. 96, 9035–9038.
Phromprasit, J., Powell, J., Assabumrungrat, S., 2016. Chem. Eng. J. 284, 1212–1223.
Radfarnia, H.R., Iliuta, M.C., 2013. Chem. Eng. J. 232, 280–289.
Raganati, F., Ammendola, P., Chirone, R., 2014. Powder Technol. 268, 347–356.
Raganati, F., Ammendola, P., Chirone, R., 2015. KONA Powder Particle J. 32, 23–40.
Rashidi, A., Yusupa, S., Loong, L.H., 2013. Chem. Eng. Trans. 35, 361–366.
Ravikovitch, P.I., Neimark, A.V., 2002. Langmuir 18, 9830–9837.
Reid, C.B., Forrester, J.S., Goodshaw, H.J., Kisi, E.H., Suaning, G.J., 2008. Ceram. Int. 34, 1551–1556.
Ridha, F., Manovic, V., Macchi, A., Anthony, E., 2015. Appl. Energy 140, 297–303.
Rouchon, L., Favergeon, L., Pijolat, M., 2013. J. Therm. Anal. Calorim. 113, 1145–1155.
Sayari, A., Belmabkhout, Y., Serna-Guerrero, R., 2011. Chem. Eng. J. 171, 760–774.
Shiri, S., Abbasi, M.H., Monshi, A., Karimzadeh, F., 2014. Adv. Powder Technol. 25, 338–341.
Smith, B., 1999. Infrared Spectra Interpretation. CRC Press, Florida.
Sun, Z., Xu, C., Chen, S., Xiang, W., 2016. Chem. Eng. J. 286, 320–328.
Suwanboon, S., Amornpitoksuk, P., Bangrak, P., 2011. Ceram. Int. 37, 333–340.
Toniolo, J.C., Takimi, A.S., Bergmann, C.P., 2010. Mater. Res. Bull. 45, 672–676.
Valverde, J.M., 2013. J. Mater. Chem. A 1, 447–468.
Valverde, J.M., Sanchez-Jimenez, P.E., Perez-Maqueda, L.A., Quintanilla, M.A.S., Pérez-Vaquero, J., 2014. Appl. Energy 125, 264–275.
Wang, K., Zhao, P., Guo, X., Han, D., Chao, Y., 2014. Energ. Convers. Manage. 86, 1147–1153.
Yang, Z., Zhao, M., Florin, N.H., Harris, A.T., 2009. Ind. Eng. Chem. Res. 48, 10765–10770.
Zamboni, I., Courson, C., Kiennemann, A., 2011. Catal. Today 176, 197–201.
Zhang, M., Peng, Y., Sun, Y., Li, P., Yu, J., 2013. Fuel 111, 636–642.

Please cite this article in press as: Granados-Pichardo, A. et al., New CaO-based adsorbents prepared by solution combustion and high-energy ball-milling processes for CO_2 adsorption: Textural and structural influences2 adsorption –>. Arabian Journal of Chemistry (2017), http://dx.doi.org/10.1016/j.arabjc.2017.03.005